

# Probing galactic double-mode RR Lyrae stars against Gaia EDR3

Geza Kovacs<sup>1</sup> and Behrooz Karamiqucham<sup>1</sup>

Konkoly Observatory, Budapest, 1121 Konkoly Thege ut. 15-17, Hungary  
e-mail: kovacs@konkoly.hu

Received April 15, 2021; accepted ??, 202?

## ABSTRACT

*Context.* Classical double-mode pulsators (RR Lyrae stars and  $\delta$  Cepheids) are important for their simultaneous pulsation in low-order radial modes. This enables us to put stringent constraints on their physical parameters.

*Aims.* We use 30 bright galactic double-mode RR Lyrae (RRd) stars to estimate their luminosities and compare these luminosities with those derived from the parallaxes of the recent data release (EDR3) of the Gaia survey.

*Methods.* We employ pulsation and evolutionary models, together with observationally determined effective temperatures to derive the basic stellar parameters.

*Results.* Excluding 6 outlying stars (e.g., with blending issues) the RRd and Gaia luminosities correlate well. With the adopted temperature zero point from one of the works based on the infrared flux method, we find it necessary to increase the Gaia parallaxes by 0.02 mas to bring the RRd and Gaia luminosities into agreement. This value is consonant with those derived from studies on binary stars in the context of Gaia. We examine also the resulting period-luminosity-metallicity (PLZ) relation in the 2MASS K band as follows from the RRd parameters. This leads to the verification of two independently derived other PLZs. No significant zero point differences are found. Furthermore, the predicted K absolute magnitudes agree within  $\sigma = 0.005\text{--}0.01$  mag.

**Key words.** Stars: fundamental parameters – stars: distances – stars: variables: RR Lyrae – stars: oscillations – stars: horizontal branch

## 1. Introduction

The historical discovery of the first double-mode RR Lyrae star, AQ Leo, in the galactic field by Jerzykiewicz & Wenzel (1977) and the subsequent discovery of 10 additional objects by Cox et al. (1983) in the globular cluster M15, opened the possibility of deriving masses of RR Lyrae stars directly from linear pulsation models, independently of stellar evolution theory. This is an important step in understanding the mass distribution of horizontal branch (HB) stars that results from the poorly known mass loss events in the thermonuclear instability phase during the final period on the first ascent to the giant branch, before falling down to the zero-age HB (ZAHB).

Double-mode pulsation (i.e., simultaneous pulsation in low-order radial modes) was known among Cepheids well before 1977 (Oosterhoff 1957a,b), and the first theoretical investigations quickly indicated a serious discrepancy between the pulsation and evolutionary masses (Petersen 1973; Stobie 1977). The solution of this discrepancy was not possible up until 1992, when stellar opacities were critically revisited by the opacity projects OPAL and OP (Iglesias & Rogers 1991, 1996; Seaton et al. 1994). These studies nicely confirmed the ‘heretic’ suggestion of Simon (1982). He recognized that an increase of several factors in the heavy element opacities should solve the ‘beat Cepheid mass discrepancy’ and also two other big issues of stellar pulsation (the excitation of  $\beta$  Cephei stars and the mass discrepancy of the bump Cepheids<sup>1</sup>).

<sup>1</sup> Assuming that the Hertzsprung progression (Hertzsprung 1926) is caused by the 2 : 1 resonance between the fundamental and 2<sup>nd</sup> overtone modes, as first suggested by Simon & Schmidt (1976) and confirmed by several subsequent studies, e.g., by Buchler et al. (1990).

Problems of similar severity for the double-mode RR Lyrae (RRd) stars did not seem to exist. Indeed, using the updated metallicities (Cox 1991; Kovacs et al. 1991, 1992) did not alter the belief that these stars are far less sensitive to even the large opacity changes predicted by OPAL/OP. This finding, is, of course, not terribly surprising, due to the overall low metallicity of RR Lyrae stars.

In spite of these encouraging events, there are several fundamental questions still left unanswered concerning double-mode pulsations both in Cepheids and RR Lyrae stars. Two issues stand out from these questions. The first one is the inability of the nonlinear hydrodynamical models to produce stationary double-mode pulsation for sound physical settings. Although there were reports in the literature of achieving this goal (Kovacs & Buchler 1993; Kolláth et al. 2002), in our view (see also Smolec & Moskalik 2010) they were more of the results of fine tuning certain parameters and accidentally catch some models that showed some level of similarity to those that are actually observed. As a result, they do not provide clear pieces of evidence for the underlying source of sustained double-mode pulsation. This failure of nonlinear hydrodynamics extends also to the no-clue nature of the (quasi-)periodic modulation of the RR Lyrae stars (known as Blazhko effect, Blazhko 1907). The second issue is the increasing number of ‘strange’ secondary periods both in Cepheids and RR Lyrae stars (Moskalik & Kolaczowski 2009; Jurcsik et al. 2015). These components, albeit with small amplitudes, are clearly identified in many cases both from space- and ground-based data. None of the radial eigenmode periods fit to the observations (Dziembowski 2016; Smolec et al. 2017). Coupled with the other unsolved dynamical issues above, we have to admit that our knowledge on the intricate physical nature of these

objects is just as limited as it was at the time when they were discovered.

Against all odds, it seems as attractive now as in the early days to assume that the ‘classical’ double-mode variables are, indeed, fundamental- (FU) and first overtone- (FO) mode pulsators and that the (highly precise) observed periods are close to the model periods derived from linear non-adiabatic (LNA) pulsation models. In this simplest form of stellar seismology, the standard approach utilizes the period – period ratio diagram (the so-called ‘Petersen’ diagram, Petersen 1973, 1978) to gain information on the stellar masses with the help of some knowledge on the heavy element metallicity, sometimes accessible by well-calibrated metallicity indicators (e.g., Preston’s  $\Delta S$  index – Preston 1959).

However, even assuming that the relative abundances of the species contributing to the overall heavy element abundance are fixed, the radial mode periods depend on four parameters: effective temperature,  $T_{\text{eff}}$ , mass  $M$ , luminosity  $L$  and metal abundance. Therefore, to aim for a more precise determination of  $M$  and  $L$  from the pulsation equations, in a series of earlier works we used also the observed color information to get a precise-enough proxy for  $T_{\text{eff}}$  (Kovacs & Walker 1999; Kovacs 2000a,b).

Verification of the stellar properties derived from double-mode variables is also very important for the consistency of the method and for the validity of the basic assumptions on the observed periods. Earlier, this check was made through the comparison with cluster/galaxy distances (Kovacs & Walker 1999; Kovacs 2000a,b) and period-luminosity-color relations based on Baade-Wesselink analyses (Dékány et al. 2008). Now, with the Early Data Release 3 (EDR3, Lindegren et al. 2021) of the Gaia mission, we have a new and exciting opportunity to verify the derived luminosities almost directly and independently of the stellar pulsation method. This approach was not feasible before EDR3, because of the factor of two or even larger errors on the DR2 parallaxes.

In this paper we investigate the compatibility of the luminosities derived from the pulsation/evolution analysis of 30 galactic field RRd stars with those computed from the EDR3 parallaxes. Furthermore, we also compare the period-luminosity-metallicity (PLZ) relation derived from the RRd pulsation with those obtained by other methods and using different datasets.

## 2. Datasets

We made a thorough search in the literature for relatively bright galactic field RRd stars with well-documented discovery analysis. We found 30 objects viable for gathering further data to conduct pulsation and stellar evolution analysis and compare the derived luminosities with those obtained from the Gaia parallaxes. Table 1 lists these stars, together with the references to the respective discovery papers.

The stars are ordered in decreasing brightness, starting with  $V = 10.8$  mag for V0500 Hya and ending with  $V = 14.4$  mag for CF Del. Most of the objects are between  $V = 12.5$  and 13.5 magnitudes. The Gaia EDR3 parallaxes peak for the two brightest stars at  $\sim 0.8$  mas and decline for the rest from  $\sim 0.4$  mas to 0.15 mas with a concomitant relative errors from 6% to 13%. The relative errors for the two brightest stars are in the ballpark of 3%, which is quite remarkable. All these show an impressive factor of two or even greater increase in the precision of the EDR3 parallaxes with respect of DR2.

To employ RRd stars in estimating their luminosities, from the observational side, we need metallicity estimates and two-color photometry, free from interstellar reddening. Unfortunately,

metallicities are not accessible for our targets. Therefore, we resort to the combination of the pulsation and stellar evolution models as described in Sect. 3. With respect to data accessibility and quality, we opt to choose the All Sky Automated Survey (ASAS, Pojmanski 1997) to estimate average magnitude in the Johnson V filter. For stars without ASAS photometry, we use Gaia photometry. To secure the  $T_{\text{eff}}$  estimate, we use the V photometry in combination with the infrared fluxes collected by the WISE satellite in the W1 and W2 bands. For the estimation of the reddening we employ the map of Schlafly & Finkbeiner (2011) accessible at the NASA IPAC site.<sup>2</sup> Additional details on the photometric datasets and the calibration methods employed are given in the following subsections.

### 2.1. The $\langle V \rangle$ magnitudes

Thanks to the large sky coverage and long-term dedication of ASAS, 26 stars from our target list have abundant time series. This allows us to perform stable Fourier fits and thereby to estimate accurately the magnitude average as the constant term  $A_0$  in the Fourier representation

$$X(t) = A_0 + \sum_{j=1}^{12} A_j \sin(2\pi\nu_j(t - t_0) + \phi_j), \quad (1)$$

where  $\{\nu_j\}$  is the linear combination of the fundamental ( $f_0$ ) and first overtone ( $f_1$ ) frequencies:  $\nu_j = |n_0 \times f_0 + n_1 \times f_1|$  with  $n_0$  and  $n_1$  satisfying the conditions  $|n_0| \geq 0$ ,  $|n_1| \geq 0$ , and  $0 < |n_0| + |n_1| \leq 3$ . In fitting Eq. 1 to the observations, first the time series  $\{V\}$  given in Johnson V magnitudes are converted to fluxes  $\{F\}$  via  $F(t) = 10^{-0.4V(t)}$ . Once  $\{F\}$  is fitted with  $\{X\}$ , the flux average  $A_0$  is converted back to magnitudes simply by setting  $\langle V \rangle = -2.5 \log A_0$ . To get a better estimate on the average, outliers in the fit are omitted at the  $3\sigma$ -level. We note that the somewhat awkward procedure of transforming magnitudes back and forth is generally employed in computing the average light level of RR Lyrae stars, because the flux averages are closer to the static stellar model values than the magnitude averages (Bono et al. 1995).

As an example of the type of time series we are dealing with, the light curve of the prototype of this class of RR Lyrae stars, AQ Leo is shown in Fig. 1. Because the two periods are incommensurate, the pulsation, strictly speaking, is non-periodic. Nevertheless, the period ratio is quite close to  $3/4$ , therefore, when folded with the beat period of 1.615 d, we get a reasonably periodic pattern. The standard deviation of the 12-component fit is 0.087 mag, which is  $\sim 50\%$  larger than the formal errors. However, the formal errors are image errors, whereas the residual scatter is time series approximation errors, and the two quantities, albeit broadly correlated, are not the same. In any case, the over 400 data points shrink the statistical error of the mean magnitude down to 0.0044 mag, which is sufficiently accurate for our purpose.

In this demonstration and throughout this work we chose the magnitudes obtained by the smallest aperture. The ASAS photometric pipeline uses 5 aperture sizes with the smallest being only 2 pixels wide (i.e.,  $30''$ , due to the large field of view of  $8.5^\circ \times 8.5^\circ$  on a  $2K \times 2K$  CCD chip.<sup>3</sup> Due to the low brightness of most of our RRd targets, blending is quite common, especially at larger apertures. Therefore, we choose the smallest aperture to minimize the effect of blending on the estimation of the average

<sup>2</sup> <https://irsa.ipac.caltech.edu/applications/DUST/>

<sup>3</sup> <http://www.astrouw.edu.pl/asas/explanations.html>

**Table 1.** The 30 galactic RRd stars analyzed in this paper

Target	Ref.	Target	Ref.	Target	Ref.	Target	Ref.	Target	Ref.
V0500 Hya	6	V5644 Sgr	6	V0374 Tel	2	V0416 Pav	3	J211848-3430.4	1
V0372 Ser	4	NN Boo	7	AZ For	2	CU Com	10	V0633 Cen	12
Z Gru	3	BS Com	3	CZ Phe	2	CR Cap	2	QW Aqr	2
XX Crv	2	V0363 Dra	8	V0338 Boo	8	AG PsA	2	J040054-4923.8	1
V0381 Tel	6	SW Ret	1	V0458 Her	8	V2493 Oph	5	J141539+0010.1	1
AQ Leo	13	AL Vol	6	XY Crv	9	BN UMa	11	CF Del	11

**Notes:** (1) [Szczygiel & Fabrycky \(2007\)](#); (2) [Bernhard & Wils \(2006\)](#); (3) [Wils \(2006\)](#) (see also authors' note on an earlier mentioning BS Com as an RRd star by [Bragaglia et al.](#)) (4) [Garcia-Melendo et al. \(2001\)](#); (5) [Garcia-Melendo, E. & Clement \(1997\)](#); (6) [Wils & Otero \(2005\)](#); (7) [Koppelman et al. \(2004\)](#); (8) [Wils et al. \(2006\)](#); (9) [Pilecki & Szczygiel \(2007\)](#); (10) [Clementini et al. \(2000\)](#); (11) [McClusky \(2008\)](#); (12) [Wils \(2010\)](#); (13) [Jerzykiewicz & Wenzel \(1977\)](#)

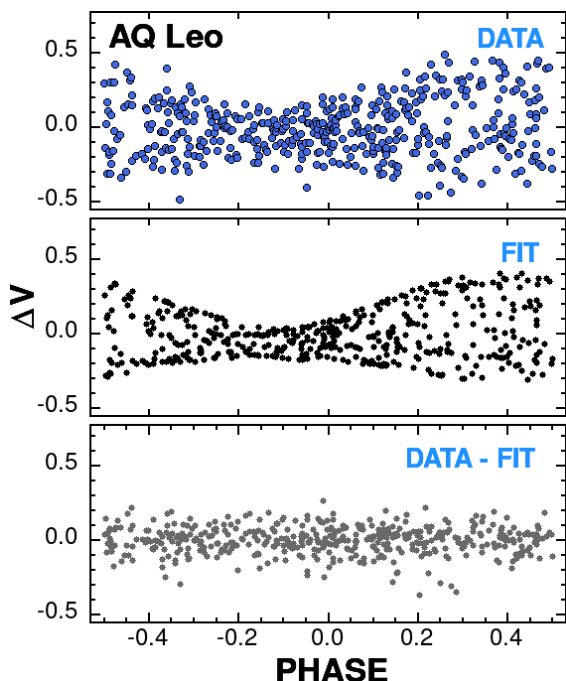


**Fig. 1.** *Upper panel:* ASAS light curve of AQ Leo folded with 1.615 d, corresponding to the beat period of the FU and FO components of the pulsation. *Middle panel:* As above but for the 3<sup>rd</sup>-order (12-component) Fourier fit given by Eq. 1. *Lower panel:* Residuals of the Fourier fit.

magnitude (even if other apertures yield light curves of lower scatter).

It is important to ensure that the derived ASAS  $\langle V \rangle$  magnitudes are compatible with high-precision observations. To test this, we rely on the recent compilation of [Monson et al. \(2017\)](#), including both archival data and new observations made by the Three-hundred MilliMeter Telescope (TMMT) of the Carnegie Observatories. By cross-matching their Table 5 and the ASAS archive, we find 22 RRab and 11 RRc stars common. The  $\langle V \rangle$  magnitudes from these two sources are plotted in Fig. 2. We see that the ASAS photometry does not show any sign of systematic offset for this relatively bright set of objects. The median differences and the mean errors are  $+0.0017 \pm 0.0045$  and  $+0.0029 \pm 0.0047$  for the FU and FO variables, respectively.

As mentioned earlier, from the 30 galactic RRd stars in our sample 26 have ASAS data available. For the remaining 4 stars we should find some way to estimate  $\langle V \rangle$ . The obvious choice may seem to be some mixture of the Gaia magnitudes in the three bands. By using the FU/FO variables of [Monson et al. \(2017\)](#), we

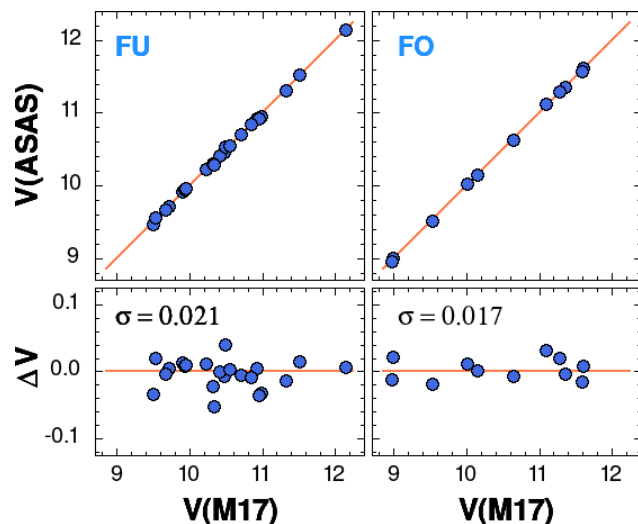


**Fig. 2.** Comparison of the ASAS average  $\langle V \rangle$  magnitudes with those of [Monson et al. \(2017\)](#). *Upper panels:*  $\langle V \rangle$  vs  $\langle V \rangle$  plots for the FU and FO variables. *Lower panels:* [Monson et al. \(2017\)](#)  $\langle V \rangle$  minus ASAS  $\langle V \rangle$  as a function of  $\langle V \rangle$  of [Monson et al. \(2017\)](#). Continuous lines indicate levels of equality.

find that this does not introduce much of an improvement in the quality of the fit as compared with the single-color fit in the BP band only. Consequently, we use a simple linear transformation of the Gaia EDR3 BP magnitudes to estimate the corresponding flux-averaged V magnitudes. It is important to emphasize that the BP magnitudes used throughout this paper are *simple averages* (i.e., not the results of Fourier fits). Therefore, as we will see below, for large-amplitude, asymmetric light curves the transformation will likely yield erroneous estimates for  $\langle V \rangle$ .

There are 18 FO variables with precise  $\langle V \rangle$  magnitudes in the paper by [Monson et al. \(2017\)](#). We add the RRd stars AQ Leo and BS Com to this set, since both have non-ASAS-based average V magnitudes ([Jerzykiewicz et al. 1982](#); [Dékány et al. 2008](#)). Because the published averages for the above two stars are magnitude averages, we subtract 0.015 from the published values to get a rough estimate on the flux-averaged V magnitude ([Bono et al. 1995](#)). We note that for a third RRd star, V0372 Ser, we have also independent, and assumed to be precise average V magnitude by [Benkő & Barcza \(2009\)](#). However, their value seem to be discordant for some reason both with the ASAS value and with the Gaia-transformed value below. Consequently, we do not use this star in deriving our calibration formula. Finally, we use 20  $\langle V \rangle$  values in the calibration of the BP magnitudes. Employing robust least squares fit, we derive the following formula

$$\langle V \rangle = 10.972 \pm 0.006 + (1.011 \pm 0.006)(BP - 11.097) . \quad (2)$$

Here we subtracted the average of BP over the sample, to have non-correlated errors on the regression coefficients. This transformation leads to a fit with  $\sigma = 0.022$  mag for the calibrating FO stars.

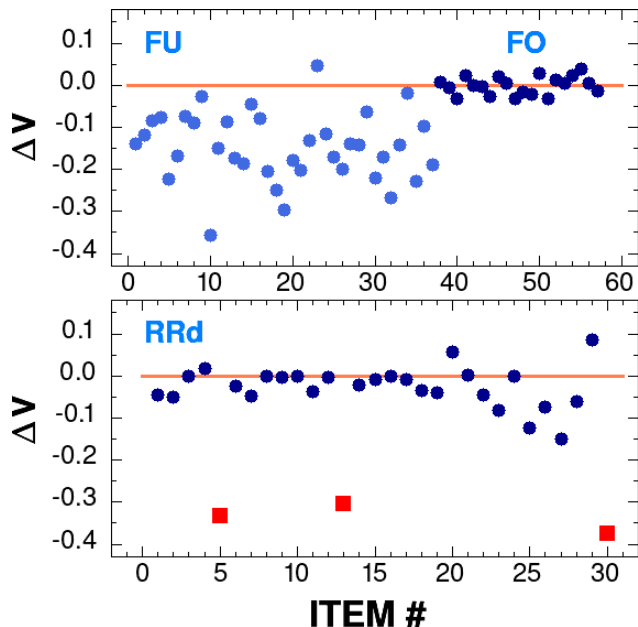


**Fig. 3.** *Upper panel:*  $\langle V \rangle$  magnitudes of Monson et al. (2017) minus those calculated from the Gaia average BP magnitude (see Eq. 2). *Lower panel:* As above but for the ASAS  $\langle V \rangle$  magnitudes of the RRd stars of this paper. Squares show the three outliers whose  $\langle V \rangle$  magnitudes are seriously flawed (most likely by blending) in the ASAS setting – see text for further details.

Figure 3 shows the striking difference between the FU and FO stars. As already mentioned above, this is primarily due to the fact that FU stars have highly non-sinusoidal light variation, and this makes the simple averages (BP average magnitudes) systematically fainter than the Fourier averages. For the RRd stars (lower panel of Fig. 3), a similar effect is observable, albeit at a much lower level. We note however, that less severe blending has the same effect, therefore, it is difficult to separate the two effects in the present case. Anyway, for the RRd stars, the overall shift remains in the range of a few hundredths of magnitude for the brighter part of our sample (the item ordering is also brightness ordering for the RRd sample). For fainter stars, the difference between the BP estimated  $\langle V \rangle$  values and those obtained directly from the ASAS data becomes larger and noisier, most likely due to the more severe blend contamination at fainter magnitudes.

We have three strong outliers among the RRd stars. The brightest star, V0381 Tel has, indeed a nearby bright companion, well within the  $15''$  radius of the smallest aperture used by ASAS. In the case of V0374 Tel we have also a crowded field with two similarly bright companions some  $20'' - 30''$  apart but it is unclear how do they affect the measured brightness of the target if we assume that the  $15''$  aperture is correctly set. One possibility is that it is positioned on the photocenter of the poorly resolved stellar triplet (target and the nearby companions), and this leads to the higher flux for the target. The faintest star, CF Del has only 34 data points in the ASAS database, leading to an inaccurate estimate of the average magnitude (the field for this target

is also crowded but the brighter companions are out of the smallest aperture we use).

In summary, according to the analysis presented in this section, we use the Fourier-based flux-averaged magnitudes of the ASAS observations for 23 stars. For the remaining  $4+3 = 7$  stars we estimate  $\langle V \rangle$  from the BP magnitudes of the EDR3 of the Gaia mission. We refer to Table A.1 for the actual values used.

## 2.2. The K magnitudes

The method employed in this paper to derive the parameters of double-mode star, requires the knowledge of the effective temperature. Thanks to the all-sky survey of the WISE infrared satellite (Wright et al. 2010), we have accurate fluxes available for all of our targets. Together with the  $\langle V \rangle$  magnitudes (as detailed in Sect. 2.1), we can use one of the numerous  $V - K \rightarrow T_{\text{eff}}$  calibrations available in the literature. In order to do that, we need to convert the WISE W1 and W2 magnitudes to K magnitudes (Johnson or 2MASS, since they differ only by an additive constant:  $K_{\text{Johnson}} = K_{2\text{MASS}} + 0.03$ )<sup>4</sup>. We find that the very recent  $K_{2\text{MASS}}$  flux-averaged magnitudes of nearly 100 galactic field RR Lyrae stars by Layden et al. (2019) and also the very recent catalog of the W1, W2 band-merged fluxes by Schlafly et al. (2019) (the unWISE catalog) suit to this task very well.

After some testing, we find that a simple linear formula does the job, and further complexities do not lead to any significant improvement. We find that the formula below fits the dereddened 2MASS magnitudes  $K_0$  of Layden et al. (2019) with a standard deviation of 0.033 mag

$$K_0 = 9.906 \pm 0.006 + (1.003 \pm 0.006)(W_0 - 9.906) . \quad (3)$$

Where  $W_0$  denotes a mixture of the dereddened unWISE magnitudes computed from the published band-merged fluxes and reddening coefficients of Wang & Chen (2019) as follows

$$\begin{aligned} W1 &= 22.5 - 2.5 \log FLUX(W1) , \\ W2 &= 22.5 - 2.5 \log FLUX(W2) , \\ (W1)_0 &= W1 - 0.121E(B - V) , \\ (W2)_0 &= W2 - 0.081E(B - V) , \\ W_0 &= 0.3(W1)_0 + 0.7(W2)_0 , \\ K_0 &= K_{2\text{MASS}} - 0.242E(B - V) . \end{aligned} \quad (4)$$

The quality of the calibration of the 98 stars is exhibited in Fig. 4. The error bars are solely from the errors of the K data, since the errors of  $\sim 0.5\%$  from the unWISE catalog are negligible. We see that, except for AR Per, all, more substantially deviating stars have large error bars. AR Per outlier status might be related to its outstandingly high reddening of  $E(B - V) = 1.110$ . By using the extinction ratios of Yuan et al. (2013) – that are some 30%–50% larger than those of Wang & Chen (2019) – only exacerbates the outlier status of this star. One possibility is that there is a high inhomogeneity in the interstellar matter in the direction of AR Per that happens to become much more transparent in an area that is not resolvable by the instrument which the map of Schlafly & Finkbeiner (2011) is based on. Another (perhaps more likely) possibility is that the foreground extinction is considerably lower than the total extinction given by the reddening map.

<sup>4</sup> See [https://old.ipac.caltech.edu/2mass/releases/second/doc/sec6\\_3.h](https://old.ipac.caltech.edu/2mass/releases/second/doc/sec6_3.h), counterchecked for this paper by the inspection of the data used in Liu & Janes (1989, 1990)

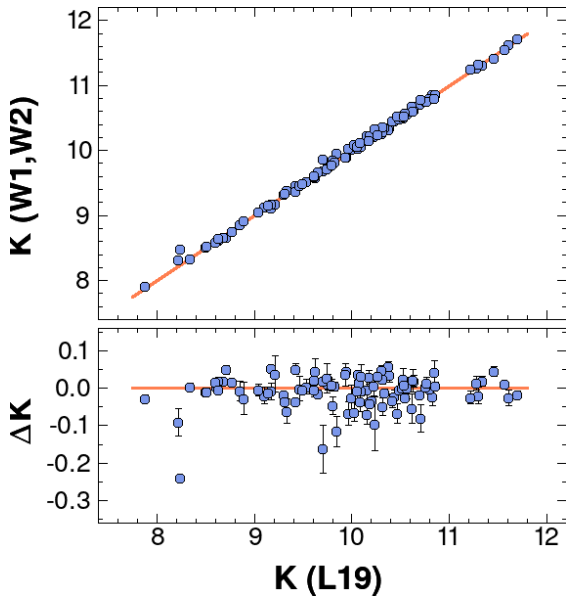


**Fig. 4.** Calibration of the unWISE (Schlafly et al. 2019) W1, W2 magnitudes to the 2MASS K magnitudes of the RR Lyrae sample of Layden et al. (2019). On the vertical axis in the upper panel, dereddened magnitudes  $K(W1, W2) = K_0$  (see Eqs. 4) are plotted. The reference levels are shown by continuous lines,  $\Delta K = K(L19) - K(W1, W2)$ . The strongest outlier in the lower panel is AR Per, with an outstandingly large reddening of  $E(B - V) = 1.110$ .

### 2.3. The $T_{\text{eff}}(V - K)$ zero point

In our earlier studies (e.g., Kovacs & Walker 1999, hereafter KW99) we used the stellar atmosphere models of (Castelli et al. 1997, hereafter C97) to relate metallicity, gravity and color to the effective temperature, with the zero point tied to the ‘generally accepted’ value based on the Infrared Flux Method (IRFM). Here we follow the same method but update the zero point by the one given for giants by González Hernández & Bonifacio (2009) (hereafter GB09).

In tying the zero point, we encounter two problems. First, the calibration of GB09 for giants is limited to  $T_{\text{eff}} < 6300$  K, with only four points above 6000 K. Therefore, the preferred  $T_{\text{eff}}$  range of  $\sim 6500 - 7000$  K of the RRd stars is basically extrapolated if one relies on the formula of GB09. Second, the formula of KW99 is linear, whereas that of GB09 is nonlinear, exposing an issue of matching the two calibrations.

The linear formula presented by KW99 matches the C97 models with a residual standard deviation (in  $\log T_{\text{eff}}$ ) better than 0.001 (corresponding to 15–20 K). The parameter range covered by the fit is as follows:  $6000 < T_{\text{eff}} < 8000$  K,  $2.5 < \log g < 3.5$ ,  $-2.5 < [M/H] < -0.5$ . Therefore, we rely on this high-quality fit concerning the parameter dependence. For matching the zero point (ZP) with that of BG09, we proceed as follows.

First we choose a set of RR Lyrae stars with reliable  $V - K$  colors and metallicities. After testing various selections from the literature, we opt the abundant sample of Dambis et al. (2013), containing 383 entries with the required number of parameters. To compare the  $T_{\text{eff}}$  estimates by the KW99 and GB09 formulae, for the KW99 formula we also need to know the gravity. For RR Lyrae stars the static gravity can be evaluated fairly well even with a limited knowledge on the stellar mass. Using a linear approximation of the type of van Albada & Baker (1971), KW99 derived the following equation from their LNA models

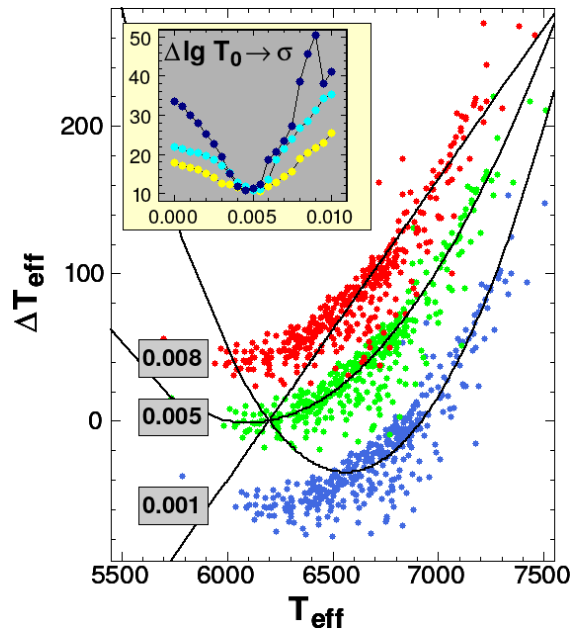


**Fig. 5.** Calibration of the ZP shift  $\Delta \log T_0$  of the  $T_{\text{eff}}$  formula (Eq. 7). The vertical axis gives  $\Delta T_{\text{eff}} = T_{\text{eff}}(\text{GB09}) - T_{\text{eff}}$ . The various ridges correspond to the ZP shifts given in the gray boxes. Continuous lines show the correction polynomial (Eq. 6) at an anchor temperature of  $T_{\text{anc}} = 6200$  K. The inset displays the RMS of the polynomial-corrected residuals as a function of the ZP shift and  $T_{\text{anc}}$  (from bottom to top, for  $T_{\text{anc}} = 6000, 6200, 6400$  K).

$$\begin{aligned} \log g &= 2.9383 + 0.2297 \log M - 0.1098 \log T_{\text{eff}} \\ &\quad - 1.2185 \log P_0 . \end{aligned} \quad (5)$$

Without introducing any significant error (at least in the present context), one can fix the stellar mass  $M$  at some ‘overall’ value. We use  $0.75 M_{\odot}$  in this particular test.

After computing the two  $T_{\text{eff}}$  estimates at any given ZP, we get a nonlinear dependence of  $\Delta T_{\text{eff}} = T_{\text{eff}}(\text{GB09}) - T_{\text{eff}}$  on  $T_{\text{eff}}$  due to the nonlinearity of the GB09 formula (see Fig. 5). Here  $T_{\text{eff}}$  denotes the KW99 fit to the atmosphere models of C97 with the ZP shift of  $\Delta \log T_0$  (see Eq. 7). To compute the RMS at any given ZP, we need to eliminate the systematic difference, entirely due to the extrapolation of the GB09 formula from the more populated, low- $T_{\text{eff}}$  regime. The rectification is made by fitting a correction polynomial of order two to  $\Delta T_{\text{eff}}$

$$\Delta T_{\text{eff}} = c_1 X + c_2 X^2, \quad X = T_{\text{eff}} - T_{\text{anc}} . \quad (6)$$

Note that we do not have adjustable constant in the above equation, since this is given as a pre-selected ZP of the KW99 formula (see below). As a result, at the anchor temperature  $T_{\text{anc}}$  no polynomial correction is made to the residual. For testing the dependence of ZP on  $T_{\text{anc}}$ , we select three anchors at the tail of the GB09 calibrating sample. The resulting ZPs should be quite independent of the actual values of these anchors.

Our  $T_{\text{eff}}$  formula with the variable ZP shift of  $\Delta \log T_0$  reads as follows

$$\begin{aligned} \log T_{\text{eff}} &= 3.9158 - \Delta \log T_0 - 0.1156(V - K) + 0.0069 \log g \\ &\quad - 0.0026[M/H] , \end{aligned} \quad (7)$$

where  $V$  and  $K$  are in the Johnson system and reddening-free. The metallicity  $[M/H]$  is assumed to be solar-scaled, so that  $[M/H] = [Fe/H] = \log Z/Z_{\odot}^*$ , with  $Z_{\odot}^* = 0.02$ .<sup>5</sup> We remind that  $K_{\text{Johnson}} = K_{2\text{MASS}} + 0.03$ .

For the anchor temperature of 6200 we illustrate the pattern of the temperature difference  $\Delta T_{\text{eff}}$  in Fig. 5. The dots of various colors correspond to the ZP shifts  $\Delta \log T_0$  as indicated in the gray boxes. All correction polynomials are zero at  $T_{\text{anc}} = 6200$  K. For incorrect ZPs these polynomials provide bad fits to  $\Delta T_{\text{eff}}$ . By scanning the possible ZPs, we end up with the plot shown in the inset. Independently of the value of  $T_{\text{anc}}$ , we conclude with the same ZP shift of  $0.0040 - 0.0055$ . Finally, we settle at  $\Delta \log T_0 = 0.0045$  in Eq. 7.

#### 2.4. The bolometric correction

Because the theoretical models work with the total irradiated flux, we need to convert the luminosity to the wave-band-limited colors to utilize the observed magnitudes in constraining the models. This is done with the intermediation of the bolometric correction BC, and can be evaluated in various ways. As in our earlier works, we opt to the stellar atmosphere models of C97 also in this study. For completeness, here we repeat the formula given in KW99 for BC with respect of the Johnson V filter

$$\begin{aligned}
BC &= 0.1924 + 0.0633u - 0.0411u^2 - 0.0233u^3 \\
&- 0.0464 \log g + 0.0689f + 0.0118f^2 - 0.0121fu \\
f &= [M/H], \quad u = c(\log T_{\text{eff}} - t) \\
c &= 2/(\log T_2 - \log T_1), \quad t = (\log T_1 + \log T_2)/2 \\
T_1 &= 6000, \quad T_2 = 8000.
\end{aligned} \tag{8}$$

This formula fits the model data with an RMS of 0.001 mag in the parameter range of interest (see Sect. 2.3). It is recalled that the zero point of this formula has been shifted by 0.113 mag with respect of the model values given by the C97 models. With this shift, the models yield  $BC_{\odot} = -0.082$ , which is very close to  $-0.07$ , following from the current bolometric and Johnson V magnitudes of the Sun by Willmer (2018). The bolometric magnitude  $M_{\text{bol}}$  of the Sun is fixed to 4.74 throughout this paper, also in agreement with Willmer (2018).

To determine the luminosity, we proceed with the well-known basic formulae

$$\begin{aligned}
M_V &= \langle V \rangle - R_V E(B - V) + 5 + 5 \log(0.001\pi) \\
\log(L/L_{\odot}) &= -0.4(M_V - M_{\text{bol}\odot} + BC),
\end{aligned} \tag{9}$$

where the symbols have their standard meanings. The parallax  $\pi$  is given in the units of milliarcsecond [mas].

### 3. Brief description of the method

The basic idea of using double-mode stars in estimating their physical properties is the same as in our earlier works (e.g., KW99). However, due to the lack of abundance measurements for the targets, we need to involve also stellar evolution models, much in the same way as we did in Dékány et al. (2008).

Concerning the pulsation models, we ran a new set of LNA models with a parameter range that is far wider than what is supposed to be occupied by the RRd stars. The model grid covers

<sup>5</sup> The C97 models refer to the then available/accepted solar heavy element abundance. This is the reason for marking  $Z_{\odot}$  by an asterisk.

**Table 2.** Parameter ranges of the pulsation models

Parameter	Range/Values	Step
Mass	0.40 – 1.00	0.05
Luminosity	30 – 100	5
$T_{\text{eff}}$	6000 – 8000	100
Z	0.00001, 0.00002, 0.00003, 0.00005	–
	0.00006, 0.00010, 0.00020, 0.00030	–
	0.00044, 0.00060, 0.00079, 0.00100	–
	0.00140, 0.00200, 0.00300, 0.01000	–

**Notes:** All models have Hydrogen abundance of 0.76.

the full instability strip and beyond. The actual LNA model grid parameters are described in Table 2. All models have 400 mass zones down to  $5 \times 10^6$  K. Although this number of zones could already provide an accurate estimates both for the period and the growth rates, nearly independently of the zoning, we followed the ‘historical’ route of arranging the mass shells, largely inherited from Stellingwerf (1975) (see also Kovacs & Buchler 1988). This implies putting 80 zones of equal mass from the surface, down to the Hydrogen ionization zone at 11000 K. The remaining zones have geometrically increasing masses down to our core boundary at  $5 \times 10^6$  K. The code we use is identical with the one used in our earlier works, i.e., all of our models have pure radiative envelopes<sup>6</sup> with the diffusion approximation, using the OPAL opacities (Iglesias & Rogers 1996).

For the stellar evolution input, we choose the recently updated models known as BaSTI<sup>7</sup> by Hidalgo et al. (2018). The models we use are Horizontal Branch (HB) models allowing evolution off the Zero Age HB up to the asymptotic giant branch. All models employed in this work are without  $\alpha$  element enhancement<sup>8</sup>, convective overshooting and diffusion. For a comparison of the grid distributions in the metallicity – mass space we show these grids for the pulsation and evolutionary models in Fig. 6. Due to the large topological sensitivity of the evolution tracks at low- to medium masses, the evolutionary models are more densely sampled for the mass in this parameter regime. For the pulsation models we do not have such an effect, therefore, they are uniformly sampled for the mass, whereas taking values near and between the pre-given metallicities by the evolution models.

Before proceeding with the description of the method of stellar parameter determination, in Fig. 7 we quickly illustrate the position of the 30 galactic RRd stars in the more customary  $P_0 - P_1 / P_0$  plane (Petersen 1973, 1978). We chose pulsation models sandwiching the metallicity range of the RRd stars to indicate the minimum and maximum metallicities allowed by the observed periods. Without posing further constraints on the pulsation models, the Petersen diagram itself gives only a very rough estimate on the stellar parameters (primarily due to the degeneracy between the metallicity and mass). Still, the arc of the observed RRd stars in the  $P_0 - P_1 / P_0$  plane clearly indicates the chemical inhomogeneity of the sample. We recall that this pat-

<sup>6</sup> Without the capability of modeling sustained double-mode pulsation, the relevance of nonlinearity and convection is unknown in the context of using periods for stellar parameter determination. Employing simple LNA periods does not seem to contradict any theoretical or observational constraint at this point.

<sup>7</sup> Bag of Stellar Tracks and Isochrones, <http://basti-iac.oa-abruzzo.inaf.it/index.html>

<sup>8</sup> Some discussion of the effect of  $\alpha$  enhancement can be found in Sect. 4.

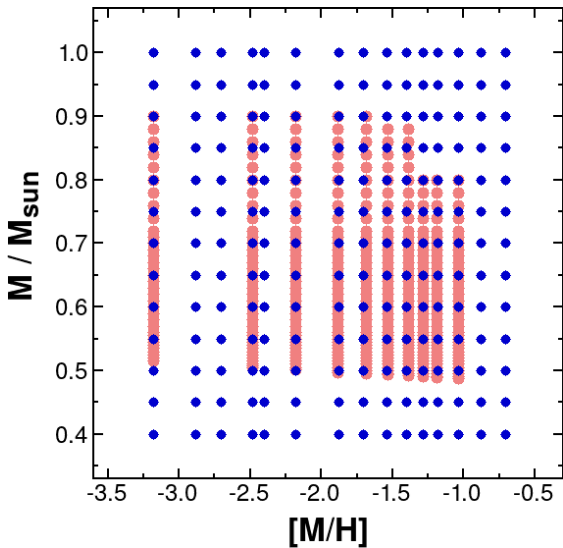


**Fig. 6.** Model metallicities vs mass for the grid values of the BaSTI stellar evolution models (light coral) and the pulsation models (blue) employed in this paper. The metallicities are scaled with  $Z_{\odot} = 0.0152$  (Caffau et al. 2011).

tern was first recognized by the MACHO Collaboration in their work on the multimode RR Lyrae inventory of the Large Magellanic Cloud (Alcock et al. 1997).

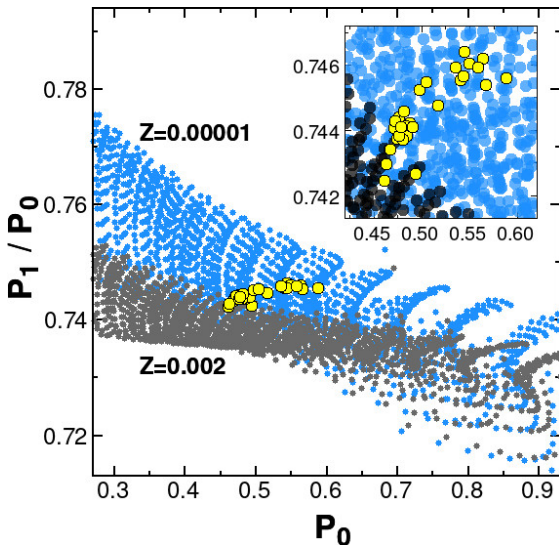


**Fig. 7.** Period – period ratio diagram for the 30 galactic RRd stars investigated in this paper (yellow filled circles). The blue and gray dots show two sets of pulsation models for the metallicity labels (corresponding to  $[M/H] = -3.18$  and  $-0.88$  if  $Z_{\odot} = 0.0152$ ). In the main plot every second models are plotted, whereas in the inset all models fitting in the constrained period regime are shown.

By using additional – observational and theoretical – pieces of information, we can place further constraints on the LNA models and arrive to a solution for the basic stellar parameters. In brief, we follow the steps below to derive the mass, luminosity and metallicity for the individual targets.

*Set input parameters:* Namely, periods of the FU and FO modes,  $P_0$  and  $P_1$ ; flux-averaged Johnson V magnitude (or, if it is not available, then Gaia BP magnitude [to be converted to Johnson V, via Eq. 2]); unWISE W1 and W2 fluxes converted to 2MASS K magnitude via Eqs. 3, 4; reddening  $E(B-V)$ .

*Select pulsation models:* Interpolate all available LNA models to the  $T_{\text{eff}}$  value, given by the input parameters and generate dense  $(M, L)$  grid from the models by quadratic interpolation on the logarithmic values. Select models satisfying the following period match constraint

$$\sqrt{\log^2\left(\frac{P_0^{\text{obs}}}{P_0^{\text{lna}}}\right) + \log^2\left(\frac{P_1^{\text{obs}}}{P_1^{\text{lna}}}\right)} < DP_{\text{max}}, \quad (10)$$

where the upper limit of the logarithmic period distance  $DP_{\text{max}}$  is set equal to 0.1%. No interpolation is made to generate a dense metallicity grid. Finally, we get a dense  $(M, L)$  grid, exactly matching the input temperature at various metallicities and periods satisfying Eq. 10.

*Select evolutionary models:* Interpolate the stellar evolution tracks linearly to the same temperature as for the pulsation models at any fixed metallicity  $Z$ . Then, generate a dense grid by interpolating the  $(M, L)$  values corresponding to this fixed temperature. As for the pulsation models, no interpolation is made for the metallicities. We end up with densely sampled model grid for  $(M, L)$ , matching the observed temperature at different metallicities.

*Matching pulsational and evolutionary models:* For the two  $(M, L)$  sets (LNA and HB evolutionary models) we can search for the closest  $(M, L)$  pairs at the same metallicity and accept as a solution by minimizing the simple distance measure given by

$$\mathcal{D}(M, L) = \sqrt{\log^2\left(\frac{L^{\text{ev}}}{L^{\text{lna}}}\right) + \log^2\left(\frac{M^{\text{ev}}}{M^{\text{lna}}}\right)}. \quad (11)$$

*Iteration on  $[Fe/H]$ :* Because the metallicity plays a role in the estimation of the input parameters (i.e.,  $T_{\text{eff}}$ , and therefore  $\log g$ ) We need to iterate on the solution to bring the starting metallicity and the one derived via Eq. 11 into close agreement. We find that within  $\sim 10$  iterations one can reach the state of consistency between the input and output metallicities.

To illustrate the method at work, in Fig. 8 we show the position of the evolutionary and pulsation models at three different metal abundances for AQ Leo, the prototype of the double-mode RR Lyrae stars. All models have the same  $T_{\text{eff}}$  of 6595 K as derived from the ASAS V and unWISE W1, W2 magnitudes. It is seen that the evolutionary and pulsational models exhibit opposite dependence on the metallicity, enabling a relatively secure selection of the metallicity range where the iso- $T_{\text{eff}}$  curves cross.

#### 4. Comparison with the Gaia EDR3 luminosities

The early version of the Gaia DR3 enables us to perform a stringent test on the luminosities we derived from the RRd stars. The Gaia luminosities are basically independent of these luminosities, since only the bolometric correction contains a dependence on  $T_{\text{eff}}$ ,  $\log g$  and  $[Fe/H]$ , entering also in the evaluation of the RRd luminosities. Errors and RRd solution dependencies play a secondary effect in the actual value of BC.

The RRd luminosities are computed for all the 30 targets as described in Sect. 3. For the evaluation of the EDR3 luminosities, we add 0.02 mas to the EDR3 parallaxes (see later in this section for some reasonings of this correction). The luminosities are compared in Fig. 9. All error sources (from BC,  $\langle V \rangle$  and parallax) are included in the vertical error bars shown as  $1\sigma$  limits for the Gaia luminosities. For the RRd luminosities the main error source is the zero point of the temperature scale. There are no other observational errors, since the periods are very accurate. However, there might be various/unknown errors in the

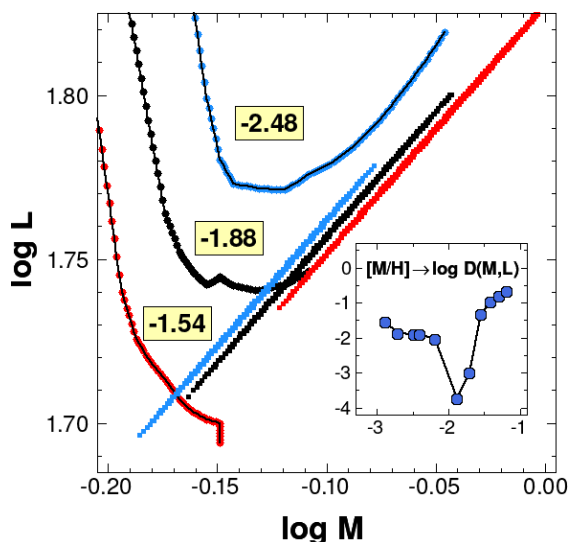


**Fig. 8.** Derivation of the mass, luminosity and metallicity of AQ Leo from the pulsational and evolutionary models. The labels show the corresponding metallicities with color coding applied also to the pulsation models. A shift of  $\pm 0.003$  in  $\log L$  is used for the pulsation models to ease the visibility of the metallicity effect (no shift for  $[M/H] = -1.88$ ,  $+0.003$  and  $-0.003$  for  $[M/H] = -2.48$  and  $-1.54$ , respectively). The inset shows the variation of the  $(M, L)$  distance metric (Eq. 11) as a function of the metallicity. All models have the same effective temperature of 6595 K, and the metallicities are scaled with  $Z_{\odot} = 0.0152$ .

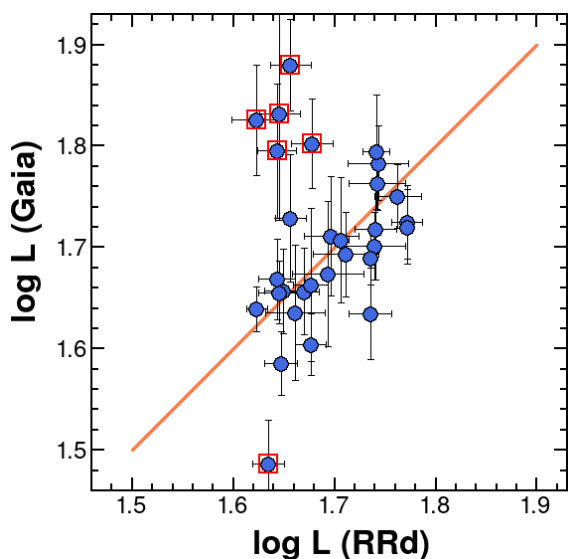


**Fig. 9.** Comparison of the luminosities derived for 30 galactic RRd stars (Tables 1, A.1) and those computed from the Gaia EDR3 parallaxes. Outliers are marked by squares and discussed in the text. For reference, the equal luminosity values are shown by the orange line.

theories we use. Since these errors are difficult to assess precisely enough, and both the evolutionary and the pulsation models proved to be quite accurate in various other applications, we pack all the possible errors in the known-to-be somewhat ambiguous zero point of  $T_{\text{eff}}$ . We compute RRd luminosities with  $\log T_{\text{eff}}$  ZPs shifted by  $\pm 0.005$  in respect of the ZP given in Sect. 2.3. Then, the horizontal error bars in the plot are given as half of the difference between the luminosities obtained with the two extreme  $\log T_{\text{eff}}$  ZPs.

We see that the two independent sets of luminosities (Gaia and RRd-based) correlate rather remarkably well if we deselect

the six outliers marked by red squares. Although parallax errors undoubtedly are good candidates to contribute to their outlier status, it is worthwhile to examine other factors, such as blending (see also Sect. 2.1). It turns out that all six objects suffer from various degrees of crowding – at least relative to the resolutions of the instruments contributing to the datasets used.<sup>9</sup> Although for CF Del and V0374 Tel we use the transformed Gaia BP magnitudes, their outlier status could not be eliminated. For the remaining four stars (V0458 Her, V5644 Sgr, SW Ret and XY Crv) we find that the ASAS photometry yields values quite close to the transformed Gaia BP magnitudes, so we use the ASAS data. After examining the WISE image stamps<sup>10</sup> for the six outliers, we find that the WISE fluxes for SW Ret, XY Crv and V0374 Tel might have been affected by close companions, if the aperture was shifted toward the photocenters.

In seeking for blend-related cause of the outlier status, it is worthwhile to recall that any systematic change in  $\langle V \rangle$  will affect both the Gaia and the RRd luminosities in a similar way. This is because we use  $V$  and  $K$  (via the unWISE magnitudes) to estimate  $T_{\text{eff}}$ . If we increase  $V$  (e.g., using Gaia photometry to cure blending), then we also increase  $V - K$  ( $K$  remains the same). As a result,  $T_{\text{eff}}$  becomes lower, yielding lower luminosity from the RRd analysis (see Fig. 3 of KW99). The higher  $\langle V \rangle$ , of course, results in a lower luminosity for the same Gaia parallax. Therefore, the status (outlier or not) does not change much by introducing changes in  $\langle V \rangle$ . The situation is different if only the infrared fluxes are influenced by blending. If corrected, this will lead to fainter  $K$  magnitude and therefore, higher  $T_{\text{eff}}$ , that is, higher RRd luminosity, i.e., weakening the outlier status. Unfortunately, this may work only for the three WISE blend candidates listed above. We conclude that it is unclear at this point what is the exact underlying cause of the outlier status of these six stars.

The derived stellar parameters of the 30 RRd stars are displayed in Table 3. The metric used to find the parameters yielding the closest match between the pulsation and evolutionary models (Eq. 11) is also given. There are 11 stars with weak matching metric, meaning basically lack of solution (i.e., lack of crossing the LNA and HBEV curves – see Fig. 8). This issue can be remedied by an increase of the  $T_{\text{eff}}$  ZP.<sup>11</sup> Indeed, with a ZP shift of  $\Delta \log T_{\text{eff}} = +0.005$  leaves only 3 stars with relative large  $DML$  values of 0.01 – 0.02. It is also noted that only some of the outliers discussed above have this type of low fidelity solution.

Using stellar evolution models with  $\alpha$  enhancement may also have some effect on the solution but it is unlikely that it acts toward the improvement of the solution. With the same total heavy element abundance,  $\alpha$  enhanced models have lower  $\log L$  by  $\sim 0.02$  (Dorman, B. 1992; Vandenberg et al. 2000). For the pulsation models the  $\alpha$  enhancement also acts in lowering both the mass and the luminosity at the same level (Kovacs et al. 1992; Kovacs & Walker 1999), so the net effect might be rather small.

Considering the still existing ambiguities in the temperature scale (Boyajian et al. 2013 – see, however, Casagrande et al. 2014), it is important to examine how the systematic shift in the Gaia parallax (as it seems necessary to employ at this point) changes as we change ZP of  $T_{\text{eff}}$ . The ZP of the IRFM/GB09-

<sup>9</sup> The resolution limits for ASAS, WISE and Gaia are  $15''$ ,  $\sim 6''$  and  $\sim 2''$ , respectively – see Sect. 2.1 and Lindegren et al. (2021); Ren et al. (2021).

<sup>10</sup> <https://irsa.ipac.caltech.edu/applications/wise/>

<sup>11</sup> The temperature increase shifts the LNA lines to higher values in the  $M-L$  plane with an opposite effect on the HBEV curves, leading to a better chance for intersecting.



**Table 3.** Derived parameters of 30 galactic RRd stars

Target	$\log L_G$	$\log T_{\text{eff}}$	$\log M$	$\log L$	[M/H]	Age	DML
V0500 Hya	$1.764 \pm 0.027$	3.8175	$-0.127 \pm 0.008$	$1.742 \pm 0.028$	$-1.88 \pm 0.50$	$61 \pm 16$	0.0003
V0372 Ser	$1.639 \pm 0.022$	3.8189	$-0.160 \pm 0.012$	$1.622 \pm 0.011$	$-1.18 \pm 0.05$	$25 \pm 14$	0.0379
Z Gru	$1.604 \pm 0.030$	3.8289	$-0.170 \pm 0.008$	$1.677 \pm 0.015$	$-1.40 \pm 0.06$	$56 \pm 24$	0.0002
XX Crv	$1.751 \pm 0.031$	3.8271	$-0.131 \pm 0.001$	$1.762 \pm 0.023$	$-2.18 \pm 0.50$	$68 \pm 02$	0.0001
V0381 Tel	$1.657 \pm 0.042$	3.8304	$-0.181 \pm 0.003$	$1.649 \pm 0.019$	$-1.18 \pm 0.11$	$40 \pm 15$	0.0003
AQ Leo	$1.783 \pm 0.037$	3.8192	$-0.117 \pm 0.010$	$1.743 \pm 0.030$	$-1.88 \pm 0.35$	$56 \pm 28$	0.0002
V5644 Sgr	$1.826 \pm 0.054$	3.8283	$-0.191 \pm 0.004$	$1.623 \pm 0.025$	$-1.04 \pm 0.12$	$48 \pm 00$	0.0060
NN Boo	$1.655 \pm 0.031$	3.8268	$-0.176 \pm 0.001$	$1.646 \pm 0.021$	$-1.18 \pm 0.11$	$30 \pm 14$	0.0069
BS Com	$1.693 \pm 0.042$	3.8327	$-0.148 \pm 0.013$	$1.711 \pm 0.032$	$-1.70 \pm 0.30$	$59 \pm 06$	0.0002
V0363 Dra	$1.701 \pm 0.033$	3.8220	$-0.127 \pm 0.011$	$1.739 \pm 0.031$	$-1.88 \pm 0.32$	$60 \pm 08$	0.0002
SW Ret	$1.487 \pm 0.043$	3.8217	$-0.166 \pm 0.007$	$1.635 \pm 0.015$	$-1.18 \pm 0.05$	$27 \pm 00$	0.0237
AL Vol	$1.690 \pm 0.027$	3.8274	$-0.129 \pm 0.020$	$1.735 \pm 0.005$	$-1.88 \pm 0.00$	$59 \pm 25$	0.0003
V0374 Tel	$1.795 \pm 0.066$	3.8243	$-0.172 \pm 0.003$	$1.643 \pm 0.019$	$-1.18 \pm 0.11$	$28 \pm 08$	0.0122
AZ For	$1.725 \pm 0.036$	3.8182	$-0.125 \pm 0.008$	$1.772 \pm 0.015$	$-2.40 \pm 0.26$	$68 \pm 05$	0.0002
CZ Phe	$1.720 \pm 0.037$	3.8196	$-0.104 \pm 0.021$	$1.772 \pm 0.005$	$-2.18 \pm 0.15$	$62 \pm 11$	0.0002
V0338 Boo	$1.669 \pm 0.040$	3.8207	$-0.174 \pm 0.005$	$1.643 \pm 0.018$	$-1.18 \pm 0.07$	$26 \pm 17$	0.0119
V0458 Her	$1.880 \pm 0.045$	3.8253	$-0.169 \pm 0.002$	$1.657 \pm 0.020$	$-1.28 \pm 0.11$	$21 \pm 16$	0.0078
XY Crv	$1.803 \pm 0.044$	3.8309	$-0.174 \pm 0.001$	$1.678 \pm 0.021$	$-1.40 \pm 0.13$	$60 \pm 23$	0.0002
V0416 Pav	$1.586 \pm 0.031$	3.8204	$-0.164 \pm 0.006$	$1.647 \pm 0.016$	$-1.18 \pm 0.05$	$26 \pm 01$	0.0175
CU Com	$1.794 \pm 0.057$	3.8207	$-0.121 \pm 0.011$	$1.741 \pm 0.013$	$-1.88 \pm 0.09$	$58 \pm 29$	0.0003
CR Cap	$1.636 \pm 0.067$	3.8281	$-0.164 \pm 0.009$	$1.661 \pm 0.029$	$-1.40 \pm 0.18$	$02 \pm 11$	0.0068
AG PsA	$1.635 \pm 0.045$	3.8305	$-0.119 \pm 0.001$	$1.735 \pm 0.021$	$-1.88 \pm 0.15$	$54 \pm 09$	0.0004
V2493 Oph	$1.657 \pm 0.042$	3.8340	$-0.168 \pm 0.008$	$1.670 \pm 0.015$	$-1.40 \pm 0.05$	$28 \pm 18$	0.0003
BN UMa	$1.711 \pm 0.059$	3.8166	$-0.144 \pm 0.007$	$1.697 \pm 0.027$	$-1.54 \pm 0.17$	$27 \pm 13$	0.0013
ASAS J211848-3430.4	$1.729 \pm 0.063$	3.8150	$-0.145 \pm 0.008$	$1.657 \pm 0.015$	$-1.40 \pm 0.06$	$24 \pm 02$	0.0275
V0633 Cen	$1.707 \pm 0.062$	3.8400	$-0.182 \pm 0.017$	$1.706 \pm 0.008$	$-1.54 \pm 0.00$	$72 \pm 09$	0.0002
QW Aqr	$1.663 \pm 0.075$	3.8328	$-0.174 \pm 0.005$	$1.677 \pm 0.017$	$-1.40 \pm 0.07$	$60 \pm 32$	0.0002
ASAS J040054-4923.8	$1.718 \pm 0.050$	3.8196	$-0.134 \pm 0.001$	$1.740 \pm 0.021$	$-1.88 \pm 0.24$	$64 \pm 08$	0.0003
ASAS J141539+0010.1	$1.674 \pm 0.072$	3.8318	$-0.155 \pm 0.016$	$1.693 \pm 0.035$	$-1.54 \pm 0.30$	$54 \pm 20$	0.0002
CF Del	$1.832 \pm 0.105$	3.8250	$-0.172 \pm 0.002$	$1.646 \pm 0.020$	$-1.18 \pm 0.11$	$29 \pm 04$	0.0103

**Notes:** – Except for the Gaia luminosities ( $L_G$ ) all errors show the variations caused by a change of  $\pm 0.005$  in  $\log T_{\text{eff}}$  as given in this table. – Mass and luminosity are in solar units, metal abundance [M/H] is given for  $Z_{\odot} = 0.0152$ , age is in Myr, and counted from the ZAHB. – The last column shows the distance of the closest points between the pulsation and evolutionary models in the  $\log L - \log M$  plane (see Eq. 11).

adjusted  $\log T_{\text{eff}}$  scale we use is 3.9113 (see Eq. 7 and subsequent text). We test three ZP shifts,  $-0.005$ ,  $0.0$  and  $+0.005$  with respect to this ZP. For each ZP shift we scan the average difference between the Gaia and RRd luminosities as a function of the parallax shift with respect of the published EDR3 values. We see from Fig. 10 that if we accept the ZP dictated by the IRFM work of González Hernández & Bonifacio (2009), then adding 0.02 mas to the published parallaxes can be considered as appropriate to bring the Gaia luminosities into agreement with the RRd luminosities. On the other hand, with an increase of  $\Delta \log T_{\text{eff}} = 0.005$  we may no need to change anything with the EDR3 parallaxes. We recall (as just mentioned) that with a higher temperature scale the match between the LNA and HBEV models becomes also much better.

Studies on various distance indicators show that the systematic bias in the published Gaia parallaxes decreased at each step of the new releases. From the period-luminosity relation of a large sample of W Uma binaries, Ren et al. (2021) derive that an overall shift of 0.029 mas of the EDR3 parallaxes (that is, adding 0.029 mas to the published parallaxes) brings them into agreement with those obtained from the standard binary star analyses. The shift differs only by 0.004 mas from the one suggested by the Gaia team (Lindgren et al. 2021). Earlier, by using the large sample of benchmark eclipsing binaries of Stassun & Tor-

res (2016), the same authors (Stassun & Torres 2021) landed at a similar conclusion, suggesting a somewhat smaller overall shift of 0.025 mas with substantial variation over the ecliptic latitude. The parallax shift derived in this paper favors the above values. However, it is important to emphasize the role of the temperature zero point (as discussed above). Both in the RRd and in the eclipsing binary analyses, a crucial point is the choice of this parameter. A sufficient upward modification may lead to complete agreement, without any parallax shift.

## 5. PLZ relation from RRd stars

Because of the increasing importance of the period-luminosity-metallicity (PLZ) relations in the past twenty or so years in the field of RR Lyrae stars, here we make a brief comparison between the PLZ resulting from the RRd stars derived in this paper for the 2MASS K band and some of the PLZs derived by other means. We note that in similar comparative work, Dékány (2009) employed 20 RRd stars (3 from the galactic field and 17 from the Large Magellanic Cloud) to compare the Wesenheit indices  $W(V, B - V)$  of these stars with those obtained from the Baade-Wesselink (B-W) analysis of 22 galactic FU stars (Kovacs 2003). The conclusion of the work of Dékány (2009) was that the  $P_0 - W(V, B - V)$  relations obtained from the RRd analysis (akin to

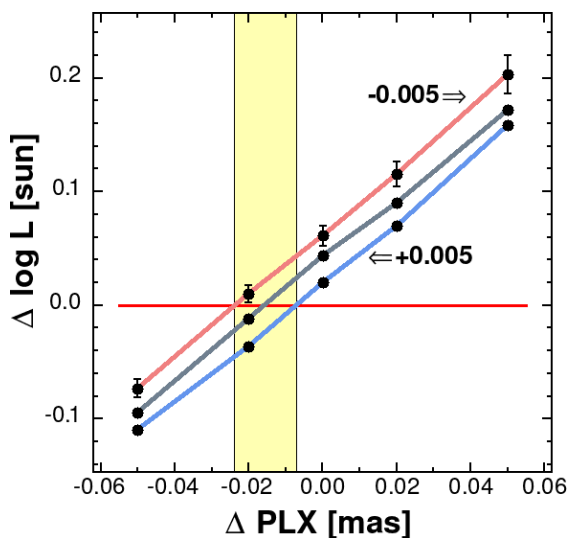


**Fig. 10.** Dependence of the average luminosity difference  $\log(\text{Gaia}) - \log(\text{RRd})$  on the parallax shift (published minus shifted) for the RRd star sample. The separate lines correspond to  $\log T_{\text{eff}}$  ZP shifts (relative to our adopted ZP as given in Sect. 2.3) of  $-0.005$ ,  $0.0$  and  $+0.005$ . Error bars show the statistical errors of the mean differences. To avoid jamming, the error bars are shown only for one  $T_{\text{eff}}$  ZP shift (others are very similar). Requesting exact equality of the luminosity averages, the shaded area indicates the range of the allowed EDR3 parallax correction.

the one presented in this paper) and from the B-W analysis were statistically consistent. However, the RRd relation turned out to be much tighter and steeper than the one resulting from the B-W analysis.

The derivation of the RRd PLZ is very straightforward. The RRd analysis yields  $P_0$ ,  $T_{\text{eff}}$ ,  $L$  and  $Z$ . Then, knowing these quantities, we can apply bolometric corrections to the luminosity values and get the visual absolute magnitude  $M_V$ . After inverting Eq. 7 for  $M_V - M_K$ , we get the absolute 2MASS  $K$  magnitude simply by subtracting  $0.03$  from  $M_K$  (see Sect. 2.2).

The resulting  $\log P_0 - K_s$  plot (where  $K_s$  denotes the 2MASS  $K$  magnitude) is shown in the upper panel of Fig. 11. As expected, the correlation is significant but the scatter is somewhat excessive. It has been long claimed and shown in several papers (e.g., Bono et al. 2003) that there is also a significant metallicity dependence for  $K_s$ . Indeed, as shown in the lower panel of Fig. 11, by regressing both the period and the metallicity, we get a considerably tighter correlation. With three relatively ‘mild’ outliers (XX Crv, AZ For and AG PsA) a robust fit yields the following formula

$$K_s = -(0.396 \pm 0.003) - (2.606 \pm 0.134)(\log P_0 + 0.30) + (0.158 \pm 0.011)([Fe/H] + 1.36) . \quad (12)$$

The standard deviation of the above regression is  $0.0086$  mag. It is interesting to examine the  $T_{\text{eff}}$  ZP issue discussed in Sect. 4 in terms of the tightness of the RRd PLZ relation. It seems that the tightness of this relation favors fairly significantly to the GB09 scale. By changing the ZP of  $\log T_{\text{eff}}$  for the three-parameter fits, we get residual standard deviations of  $0.025$  and  $0.043$  magnitudes for  $\Delta \log T_{\text{eff}} = -0.005$  and  $+0.005$ , respectively. This result seems to contradict to the higher temperature scale suggested by the better HBEV/LNA match accuracy of the models and further supports the need for the correction of the Gaia paral-

axes.<sup>12</sup> Nevertheless, it is unclear how tight the true PLZ should be. There is a hidden mass and temperature dependence in the PLZ relation, and it is not entirely known how much evolutionary and color effects make these parameters correlated with each other, and thereby tighten the observed PLZ relation.

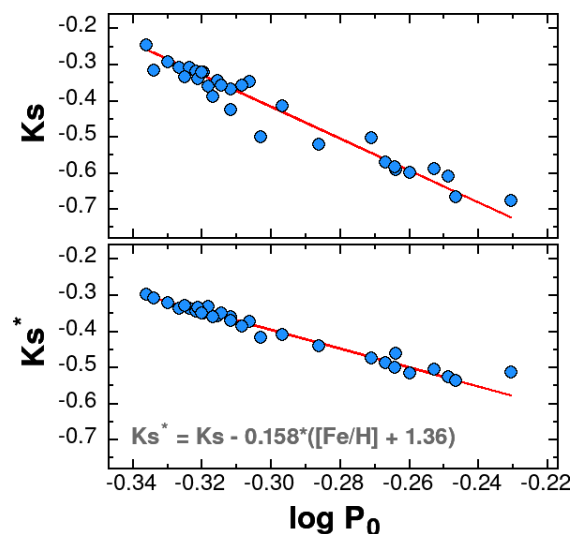


**Fig. 11.** Upper panel: Absolute  $K_s$  magnitudes derived from pulsation and evolution models for the 30 galactic RRd stars of Table 1 as a function of the fundamental period. Lower panel: As above, but for the modified  $K_s$  values for the metallicity effect. Continuous lines show the respective regressions (see Eq. 12 for the fit shown in the lower panel).

In a comparison with other, recent variants of the RR Lyrae PLZ relation, we choose the relation of Marconi et al. (2015), based on pulsation and stellar evolution considerations, and that of Neeley et al. (2019) from the purely empirical fit to the bright, single-mode RR Lyrae stars with high-fidelity Gaia (DR2) parallaxes. The PLZ relations are compared in Fig. 12. The agreement is very good between all these independent estimates with tighter but systematically more deviating trend for the relation based on the Gaia DR2 parallaxes. In a comparison of the regression coefficients (see Table 4), we see that although our formula seems to be closer to that of Neeley et al. (2019) the systematic trend is stronger than for the formula of Marconi et al. (2015). This underlines the significance of the metallicity term, that is stronger in both of these formulae than in ours. This is partially compensated by the weaker period dependence in the formula of Marconi et al. (2015) but works in the opposite way with the strong period dependence derived by Neeley et al. (2019). In spite of these details, likely due to the errors of the fits, we think that the overall agreement with standard deviations of  $0.005$ – $0.01$  mag is very satisfying between the different approximations.

## 6. Conclusions

The steadily improving accuracy of the Gaia parallaxes allows us to visit increasing number of objects and derive various physical parameters with impressively high precision. RR Lyrae stars are among those objects that come into the forefront of investigation, due to their significance in galactic structure and stellar

<sup>12</sup> In a current paper on single-mode galactic RR Lyrae stars Marconi et al. (2021) conclude that the parallax correction might be statistically insignificant. However, it seems that their data are too noisy to detect the small parallax shift claimed by other studies.

**Table 4.** Comparison of the PLZ regression coefficient

a	b	c	Source
-0.390	-2.250	+0.180	Marconi et al. (2015)
-0.390	-2.730	+0.180	Neeley et al. (2019)
-0.396	-2.606	+0.158	this paper

**Note:** The coefficients refer to the following type of formula:  
 $K_s = a + b(\log P_0 + 0.30) + c([\text{Fe}/\text{H}] + 1.36)$

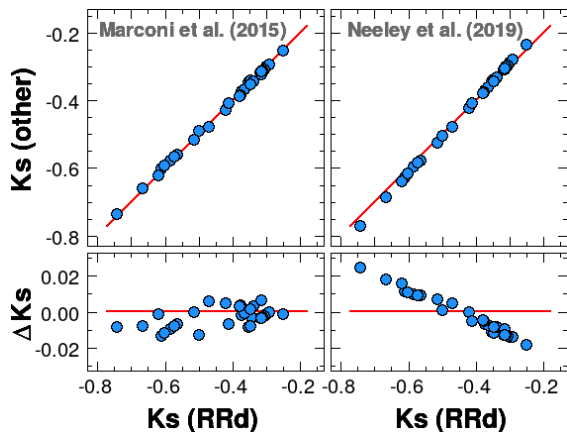


**Fig. 12.** Comparison of the PLZ relations as given in Table 4. All formulae are compared on the set of  $(\log P_0, [\text{Fe}/\text{H}])$  values given in Table 3. The lower panels show the differences  $\Delta K_s = K_s(\text{RRd}) - K_s(\text{other})$  between the pair of formulae.

evolution. In this paper we used relatively bright galactic double-mode RR Lyrae (RRd) stars and confronted their (largely) theoretical luminosities with those obtained (almost) directly from their parallaxes currently made available by the third (early) data release (EDR3) of the Gaia mission. With almost all individual parallax errors less than 10%, and sample size of 30, it is possible to aim for few percent statistical precision in defining the zero point of the RR Lyrae luminosity scale and investigate the source of the remaining systematic differences.

We implemented a very similar method to those used in our earlier investigations. The method is based on the simple observation that the two periods yield a closed solution for the stellar parameters, assuming that we have reliable estimates on the temperature and metallicity. Unfortunately, for the stars under scrutiny, the latter quantity is unavailable, therefore we had to resort to the combination of pulsation and evolutionary models (BaSTI, Hidalgo et al. 2018), together with observationally determined temperature much in the same way as in Dékány et al. (2008). In return, this method yields a full solution, including an estimate on the metallicity. Our main results are as follows.

- Except for 6 outlying stars (likely affected by blending and parallax errors), the luminosities of the remaining 24 stars correlate well with those derived from the Gaia EDR3 parallaxes.
- By fixing the  $T_{\text{eff}}$  zero point to the one given by González Hernández & Bonifacio (2009), we get no systematic differences between the Gaia and RRd luminosities, assuming that the Gaia parallaxes are shifted by 0.02 mas upward. This result is consonant with other studies suggesting similar (albeit some 0.005–0.01 mas larger) corrections.
- We derived a period-luminosity-metallicity (PLZ) relation for the 2MASS K color, and found that it is in good agreement with two other, independent PLZ relations. The first

relation (Neeley et al. 2019) is based on direct Gaia DR2 distances, whereas the second (Marconi et al. 2015) comes from pulsation-stellar evolution considerations. Our PLZ relation is fundamentally theoretical, aided by the observationally calibrated zero point of  $T_{\text{eff}}$ . There are no significant differences in the zero points and the predicted values have a scatter (standard deviation) of only  $\sim 0.01$  mag.

- The tightness criterion of the RRd PLZ relation significantly favors the  $T_{\text{eff}}$  zero point accepted for this study. This lends further support to the upward correction of the EDR3 parallaxes as mentioned above.

The work presented in this paper would have been much simpler, and independent of stellar evolutionary models, if we had reliable metal abundances available for our targets. By knowing the metallicity and the temperature, one can estimate the luminosity using only pulsation theory and directly compare these values with the Gaia luminosities, without the intermediary of the evolutionary models. The future availability of metallicity for bright double-mode variables, and, in particular, for RR Lyrae stars, is an important step for a nearly direct test of the Gaia parallaxes and evolutionary models.

*Acknowledgements.* It is a pleasure to thank to Andy Monson for the valuable correspondence on the calibration of the photometric data used in this paper. This work is based heavily on the availability of well-calibrated photometry of the All Sky Automated Survey (ASAS). We thank to Grzegorz Pojmanski and his co-workers for running this great project for so many years. This research has made use of the VizieR catalogue access tool, CDS, Strasbourg, France (DOI: 10.26093/cds/vizier). This work has made use of data from the European Space Agency (ESA) mission *Gaia* (<https://www.cosmos.esa.int/gaia>), processed by the *Gaia* Data Processing and Analysis Consortium (DPAC, <https://www.cosmos.esa.int/web/gaia/dpac/consortium>). Funding for the DPAC has been provided by national institutions, in particular the institutions participating in the *Gaia* Multilateral Agreement. This publication makes use of data products from the Wide-field Infrared Survey Explorer, which is a joint project of the University of California, Los Angeles, and the Jet Propulsion Laboratory/California Institute of Technology, funded by the National Aeronautics and Space Administration. This research has made use of the NASA/IPAC Infrared Science Archive, which is funded by the National Aeronautics and Space Administration and operated by the California Institute of Technology. This research has made use of the International Variable Star Index (VSX) database, operated at AAVSO, Cambridge, Massachusetts, USA. Supports from the National Research, Development and Innovation Office (grants K 129249 and NN 129075) are acknowledged.

## References

- Alcock, C., Allsman, R. A., Alves, D. et al. 1997, *ApJ*, 482, 89  
 Benkő, J. M. & Barcza, Sz. 2009, *A&A*, 497, 481  
 Bernhard, K. & Wils, P. 2006, *IBVS*, No. 5698  
 Blazhko, S. 1907, *Astr. Nachr.*, 175, 325  
 Bono, G., Caputo, F., Castellani, V. et al. 2003, *MNRAS*, 344, 1097  
 Bono, G., Caputo, F., Stellingwerf, R. F. 1995, *ApJS*, 99, 263  
 Boyajian, T. S., von Braun, K., van Belle, G. et al. 2013, *ApJ*, 771, 40  
 Buchler, J. R., Moskalik, P., Kovacs, G. 1990, *ApJ*, 351, 617  
 Caffau E., Ludwig H.-G., Steffen M. et al. 2011, *Sol. Phys.*, 268, 255  
 Casagrande, L., Portinari, L., Glass, I. S. et al. 2014, *MNRAS*, 439, 2060  
 Castelli, F., Gratton, R. G., Kurucz, R. L. 1997, *A&A*, 318, 841  
 Clementini, G., Di Tomaso, S., Di Fabrizio, L. et al. 2000, *AJ*, 120, 2054  
 Cox, A. N., Hodson, S. W., Clancy, S. P. 1983, *ApJ*, 266, 94  
 Cox, A. N. 1991, *ApJ*, 381, L71  
 Dambis, A. K., Berdnikov, L. N., Kniazev, A. Y. et al. 2013, *MNRAS*, 435, 3206  
 Dékány, I., Kovacs, G., Jurcsik, J. et al., 2008, *MNRAS*, 386, 521  
 Dékány, I. 2009, *AIPC*, 1170, 245  
 Dorman, B. 1992, *ApJS*, 81, 221  
 Dziembowski, W. A. 2016, *CoKon*, 105, 23  
 Garcia-Melendo, E. & Clement, Ch. M. 1997, *AJ*, 114, 1190  
 Garcia-Melendo E., Henden A. A., Gomez-Forellad, J. M. 2001, *IBVS*, No. 5167  
 González Hernández, J. I. & Bonifacio, P. J. I. 2009, *A&A*, 497, 497  
 Hertzprung, E. 1926, *Bull. Astr. Inst. Netherlands*, 3, 115  
 Hidalgo, S. L., Pietrinferni, A., Cassisi, S. et al. 2018, *ApJ*, 856, 125

- Iglesias, C. A. & Rogers, F. J. 1991, *ApJ*, 371, L73  
Iglesias, C. A. & Rogers, F. J. 1996, *ApJ*, 464, 943  
Jerzykiewicz, M. & Wenzel, W. 1977, *Acta Astronomica*, 27, 35  
Jerzykiewicz, M., Schult, R. H., Wenzel, W. 1982, *Acta Astronomica*, 32, 358  
Jurcsik, J., Smitola, P., Hajdu, G. et al. 2015, *ApJS*, 219, 25  
Kolláth, Z., Buchler, J. R., Szabó, R. et al. 2002, *A&A*385, 932  
Koppelman, M. D., Wils, P., Welch, D. L., Durkee, R., Vidal-Sáinz, J. 2004, American Astronomical Society Meeting 205, id.54.05; *Bulletin of the American Astronomical Society*, 36, 1428  
Kovacs, G. & Buchler, J. R. 1988, *ApJ*, 324, 1026  
Kovacs, G., Buchler, J. R., & Marom, A. 1991, *A&A*, 252, L27  
Kovacs, G., Buchler, J. R., Marom, A., et al. 1992, *A&A*, 259, L46  
Kovacs, G. & Buchler, J. R. 1993, *ApJ*, 404, 765  
Kovacs, G. & Walker, A. R. 1999, *ApJ*, 512, 271  
Kovacs, G. 2000a, *A&A*, 360, L1  
Kovacs, G. 2000b, *A&A*, 363, L1  
Kovacs, G. 2003, *MNRAS*, 342, L58  
Layden, A. C., Tiede, G. P., Chaboyer, B. et al. 2019, *AJ*, 158, 105  
Lindegren, L., Klioner, S. A., Hernández, J. et al. 2021, *A&A*, accepted (arXiv:2012.03380)  
Liu, T. & Janes, K. A. 1989, *ApJS*, 69, 593  
Liu, T. & Janes, K. A. 1990, *ApJ*, 354, 273  
Longmore, A. J., Dixon, R. I., Buckley, D. R. V. 1990, *ASPC*, 11, 36  
McClusky, J. V. 2008, *IBVS*, No. 5825  
Marconi, M., Coppola, G., Bono, G. et al. 2015, *ApJ*, 808, 50  
Marconi, M., Molinaro, R., Ripepi, V. et al. 2021, *MNRAS*, 500, 5009  
Monson, A. J., Beaton, R. L., Scowcroft, V., et al. 2017, *AJ*, 153, 96  
Moskalik, P. & Kolaczowski, Z. 2009, *MNRAS*, 394, 1649  
Neeley, J. R., Marengo, M., Freedman, W. L. et al. 2019, *MNRAS*, 490, 4254  
Oosterhoff, P. Th. 1957a, *Bulletin of the Astron. Inst. of the Neth.*, 13, 317  
Oosterhoff, P. Th. 1957b, *Bulletin of the Astron. Inst. of the Neth.*, 13, 320  
Petersen, J. O., 1973, *A&A*, 27, 89  
Petersen, J. O., 1978, *A&A*, 62, 205  
Pilecki, B. & Szczygiel, D. M. 2007, *IBVS*, No. 5785  
Pojmanski, G. 1997, *ã*, 47, 467  
Preston, G. W. 1959, *ApJ*, 130, 507  
Ren, F., Chen, X., Zhang, H. et al. 2021, *ApJ*, accepted (arXiv:2103.16096v1)  
Schlafly, E. F. & Finkbeiner, D. P., 2011, *ApJ*, 737, 103  
Schlafly, E. F., Meisner, A. M., Green, G. M. 2019, *ApJS*, 240, 30  
Seaton, M. J., Yan, Y., Mihalas, D. et al., 1994, *MNRAS*, 266, 805  
Simon, N. R. & Schmidt, E. 1976, *ApJ*, 205, 162  
Simon, N. R. 1982, *ApJ*, 260, L87  
Smolec, R. & Moskalik, P. 2010, *A&A*, 524, A40  
Smolec, R., Dziembowski, W., Moskalik, P. et al. 2017, *EPJWC*, 152, 06003  
Stassun, K. G. & Torres, G. 2016, *ApJ*, 831, L6  
Stassun, K. G. & Torres, G. 2021, *ApJ*, 907, L33  
Stellingwerf, R. F. 1975, *ApJ*, 195, 441  
Stobie, R. S. 1977, *MNRAS*, 180, 631  
Szczygiel, D. M. & Fabrycky, D. C. 2007, *MNRAS*, 377, 1263  
van Albada, T. S. & Baker, N. 1971 *ApJ*, 169, 311  
VandenBerg, D. A., Swenson, F. J., Rogers, F. J. et al. 2000, *ApJ*, 532, 430  
Wang, S., Chen, X. 2019, *ApJ*, 877, 116  
Willmer, Christopher, N. A. 2018, *ApJS*, 236, 47  
Wils, P. & Otero, S. A. 2005, *IBVS*, No. 5593  
Wils, P. 2006, *IBVS*, No. 5685  
Wils, P., Lloyd, C., Bernhard, K. 2006, *MNRAS*, 368, 1757  
Wils, P. 2010, *IBVS*, No. 5955  
Wright, E. L., Eisenhardt, P. R. M., Mainzer, A. K. et al. 2010, *AJ*, 140, 1868  
Yuan, H.B., Liu, X.W., Xiang, M.S. 2013, *MNRAS*, 430, 2188

## Appendix A: Observational datasets used in this work

We summarize the observational data used in this study in Table A.1. The discoveries and the periods were reported by the papers listed in Table 1. The flux-averaged magnitudes in the Johnson V filter are based on the 3<sup>rd</sup>-order Fourier fit (see Sect. 2.1) to the ASAS V observations by starting from the published periods and refining them due to the long time span of the ASAS data. Four entries (marked by double asterisks) do not have ASAS light curves, therefore their  $\langle V \rangle$  values were approximated with the aid of the Gaia photometry, as described in Sect. 2.1. The same procedure was employed on three more stars (V0381 Tel, V0374 Tel, CF Del), where blending and sparse light curve sampling corrupted the ASAS magnitudes.

For completeness, the flux-averaged Gaia EDR3 magnitudes are listed for all three bands, even though we use only the BP magnitudes. For the ASAS  $\langle V \rangle$  values we take a flat error of 0.005 mag for all entries, whereas for those derived from the Gaia average fluxes, we give the errors as given by the EDR3 catalog.

The W1, W2 fluxes come from the recent unWISE catalog by Schlafly et al. (2019) and result from the band-integrated fluxes throughout the full mission of the satellite. The reddening values are from the map of Schlafly & Finkbeiner (2011) accessible from the NASA/IPAC Infrared Science Archive. Parallaxes are from the Gaia EDR3 catalog (accessed from the VizieR database).

**Table A.1.** Observed properties of 30 Galactic RRd stars

Target	$P_0$ (d)	$P_1/P_0$ (d)	$\langle V \rangle$ (mag)	G (mag)	BP (mag)	RP (mag)	W1 (flux)	W2 (flux)	E(B-V) (mag)	PLX (mas)
V0500_Hya	0.563906	0.746204	10.772	10.729	10.945	10.382	138300	136290	0.020	0.8453
	0.000000	0.000000	0.005	0.008	0.025	0.017	58	121	0.001	0.0264
V0372_Ser	0.471349	0.744098	11.320	11.268	11.492	10.872	95313	93210	0.073	0.8083
	0.000000	0.000000	0.005	0.011	0.041	0.025	49	103	0.008	0.0204
Z_Gru	0.487995	0.744243	12.340	12.281	12.450	11.958	30145	29373	0.022	0.4794
	0.000000	0.000000	0.005	0.011	0.035	0.022	28	63	0.001	0.0170
XX_Crv	0.544515	0.746429	12.375	12.282	12.468	11.921	32925	32660	0.058	0.4220
	0.000000	0.000000	0.005	0.007	0.025	0.016	30	67	0.004	0.0156
V0381_Tel**	0.467819	0.743418	12.782	12.711	12.887	12.378	20806	20358	0.041	0.3724
	0.000000	0.000000	0.032	0.009	0.032	0.020	25	56	0.001	0.0178
AQ_Leo	0.549751	0.746063	12.530	12.470	12.662	12.119	27604	26799	0.022	0.3571
	0.000000	0.000000	0.005	0.009	0.030	0.019	28	63	0.001	0.0155
V5644_Sgr	0.461258	0.74248	12.546	12.465	12.701	12.064	33528	32767	0.130	0.3884
	0.000000	0.000000	0.005	0.012	0.042	0.026	31	69	0.005	0.0249
NN_Boo**	0.474600	0.743742	12.683	12.619	12.790	12.304	21747	21172	0.013	0.3760
	0.000000	0.000000	0.025	0.008	0.025	0.016	24	53	0.001	0.0130
BS_Com	0.487902	0.744121	12.734	12.672	12.842	12.370	19897	19455	0.012	0.3513
	0.000000	0.000000	0.005	0.007	0.023	0.014	23	53	0.000	0.0175
V0363_Dra**	0.540800	0.745562	12.768	12.672	12.874	12.342	21960	21378	0.027	0.3533
	0.000000	0.000000	0.027	0.008	0.027	0.017	23	49	0.000	0.0133
SW_Ret	0.476624	0.744425	12.805	12.727	12.948	12.375	22989	22492	0.060	0.4681
	0.000000	0.000000	0.005	0.006	0.020	0.012	24	52	0.006	0.0234
AL_Vol	0.517218	0.744781	12.806	12.691	12.914	12.306	25243	24770	0.107	0.3951
	0.000000	0.000000	0.005	0.007	0.025	0.015	25	53	0.003	0.0126
V0374_Tel**	0.479065	0.743866	13.193	13.102	13.294	12.737	15586	15079	0.053	0.2628
	0.000000	0.000000	0.045	0.012	0.044	0.026	22	50	0.001	0.0203
AZ_For	0.588230	0.745627	12.894	12.814	13.020	12.489	19462	18999	0.012	0.3178
	0.000000	0.000000	0.005	0.006	0.019	0.012	23	52	0.000	0.0137
CZ_Phe	0.566809	0.745392	12.898	12.812	13.010	12.490	19153	18580	0.011	0.3178
	0.000000	0.000000	0.005	0.006	0.021	0.013	23	51	0.001	0.0140
V0338_Boo**	0.494040	0.742673	12.959	12.860	13.063	12.546	17847	17309	0.015	0.3258
	0.000000	0.000000	0.031	0.009	0.031	0.020	22	47	0.001	0.0149
V0458_Her	0.483740	0.74416	13.123	13.027	13.233	12.681	16715	16213	0.058	0.2470
	0.000000	0.000000	0.005	0.007	0.021	0.013	22	49	0.002	0.0136
XY_Crv	0.484820	0.743851	13.311	13.247	13.445	12.872	14432	13971	0.082	0.2565
	0.000000	0.000000	0.005	0.008	0.028	0.018	21	50	0.003	0.0137
V0416_Pav	0.491515	0.74411	13.347	13.259	13.485	12.859	15270	15066	0.091	0.3348
	0.000000	0.000000	0.005	0.006	0.022	0.014	21	49	0.004	0.0124
CU_Com	0.544164	0.745659	13.363	13.227	13.406	12.907	12603	12232	0.020	0.2324
	0.000000	0.000000	0.005	0.008	0.028	0.018	19	47	0.001	0.0161
CR_Cap	0.473022	0.744283	13.366	13.290	13.464	12.960	12249	12013	0.036	0.2866
	0.000000	0.000000	0.005	0.009	0.030	0.019	20	50	0.001	0.0230
AG_PsA	0.497841	0.745248	13.379	13.342	13.522	13.027	11494	11130	0.018	0.2786
	0.000000	0.000000	0.005	0.009	0.034	0.022	19	46	0.002	0.0151
V2493_Oph	0.463324	0.742977	13.482	13.403	13.661	12.980	14068	13720	0.140	0.3079
	0.000000	0.000000	0.005	0.008	0.028	0.017	20	47	0.009	0.0156
BN_UMa**	0.535786	0.745932	13.580	13.504	13.677	13.172	10359	10168	0.014	0.2292
	0.000000	0.000000	0.030	0.009	0.030	0.019	18	43	0.002	0.0162
J211848-3430.4	0.504860	0.745486	13.653	13.597	13.870	13.156	12492	12231	0.101	0.2472
	0.000000	0.000000	0.005	0.009	0.032	0.020	20	48	0.004	0.0190
V0633_Cen	0.480517	0.743739	13.621	13.588	13.790	13.233	9865	9738	0.076	0.2449
	0.000000	0.000000	0.005	0.012	0.044	0.027	17	43	0.002	0.0184
QW_Aqr	0.477237	0.743836	13.705	13.715	13.949	13.308	10235	10038	0.098	0.2564
	0.000000	0.000000	0.005	0.010	0.036	0.024	18	45	0.006	0.0235
J040054-4923.8	0.558588	0.745934	13.824	13.768	13.977	13.453	7994	7825	0.007	0.1992
	0.000000	0.000000	0.005	0.008	0.028	0.017	15	35	0.001	0.0123
J141539+0010.1	0.481932	0.744591	13.873	13.737	13.882	13.419	7552	7263	0.035	0.2114
	0.000000	0.000000	0.005	0.010	0.035	0.023	16	40	0.001	0.0187
CF_Del**	0.478448	0.74411	14.348	14.217	14.436	13.845	5880	5709	0.087	0.1471
	0.000000	0.000000	0.030	0.009	0.030	0.019	14	38	0.001	0.0196

**Notes:** The lines below the entry lines show the corresponding errors. The  $\langle V \rangle$  values derived from the calibration of the EDR3 BP magnitudes (see Eq. 2) are marked by \*\*.